Quantum-beat spectroscopy of image-potential resonances

M. Marks,[1] C. H. Schwalb,[1] K. Schubert,[1] J. Güdde,[1] and U. Höfer[1,2]
[1]*Fachbereich Physik und Zentrum für Materialwissenschaften, Philipps-Universität, DE-35032 Marburg, Germany*
[2]*Donostia International Physics Center (DIPC), ES-20018 San Sebastián, Spain*
(Received 16 September 2011; revised manuscript received 15 November 2011; published 7 December 2011)

The dynamics of electrons in image-potential resonances on the Ag(111) surface, i.e., image-potential states that are resonant with bulk bands, have been studied by time-resolved two-photon photoemission in combination with quantum-beat spectroscopy. Energies and lifetimes of these resonances were determined up to a quantum number $n = 7$. Both quantities show a hydrogen-like scaling with quantum number n. The measured decay time of the first image-potential state ($n = 1$), which is still located in the projected band gap, is 31.5(1.5) fs. The decay time decreases to 23(2) fs for the resonance $n = 2$ and then increases up to 1 ps for $n = 7$. It is concluded that the elastic decay of the resonances due to elastic electron transfer into the bulk is nearly one order of magnitude faster than the inelastic electron-hole pair decay. Nevertheless, the elastic decay is found to be slower than theoretically predicted. The pure dephasing times of the resonances $n = 3$–7 are longer than the decay times. This suggests that electron-phonon scattering is weak despite a large bulk penetration of the resonance wave functions.

DOI: 10.1103/PhysRevB.84.245402 PACS number(s): 73.20.−r, 78.47.jm, 79.60.−i

I. INTRODUCTION

The dynamics of electron transfer processes at surfaces and interfaces plays an important role for many phenomena as, for example, chemisorption of atoms or molecules, electronically induced chemical reactions, molecular electronics as well as for scanning tunneling microscopy. In all these phenomena, electronic excitations populate initially unoccupied electronic states that can be classified into two fundamentally different types: (i) states that are located in the forbidden gap of the solid and whose decay is governed by inelastic many-body processes, e.g., electron-hole-pair excitation or electron-phonon coupling, and (ii) states that are resonant with electronic bulk bands. Electronic excitations in such quasistationary states (resonances) can additionally decay elastically due to energy-conserving resonant electron transfer into the bulk, a process that is expected to dominate over inelastic decay.[1–3] Although resonant elastic electron transfer is of great importance for many practical applications, it is still not yet well understood on a microscopic level. In contrast to that, the understanding of inelastic decay processes at surfaces is much better developed. A particularly detailed picture of the inelastic electron dynamics for states in the gap has been attained by studying the relative simple quasi-one-dimensional model system of image-potential states on metal surfaces.[4,5] Time-resolved two-photon photoemission (2PPE) experiments and accurate many-body calculations have led to a good understanding of many aspects of the inelastic decay of these initially unoccupied states.[6] On most of the metal surfaces studied so far, the image-potential states are confined in front of the surface between the attractive image-potential on the vacuum side and the repulsion from the forbidden gap on the metal side. In this quantum well, the image-potential states form a Rydberg-like series which converges to the vacuum energy E_{vac}. The projected bulk band gap of the metal limits the penetration of excited electrons into the bulk, which results in rather long inelastic lifetimes of image-potential states compared to bulk excitations with comparable excitation energies. On surfaces on which E_{vac} is located outside a projected bulk band gap, the image-potential states become degenerate with projected bulk bands and are in fact electronic resonances. This opens the possibility to study resonant charge transfer at surfaces but to retain the simple hydrogenic character of image-potential states.

In this contribution, we present a systematic investigation of the decay dynamics of a whole series of image-potential resonances on the Ag(111) surface. Similar to Cu(111) the vacuum energy E_{vac} of the Ag(111) surface is located slightly above the upper edge of the surface-projected sp band gap and the Rydberg series of image-potential states becomes degenerate with surface-projected bulk bands. Close to the $\bar{\Gamma}$ point, only the first image-potential state ($n = 1$) is located within the projected band gap as depicted in Fig. 1(a). Previous experiments on Ag(111) and Cu(111) have shown that the different character of the second image-potential state is reflected in its shorter lifetime compared to the $n = 1$ state.[9–13] The difference in the decay dynamics between gap states and resonances was also investigated in our recent 2PPE study on Cu(111) where we have used rare gases adsorption in order to shift the $n = 1$ state above the projected band gap.[14] The decay of higher members of a series of resonances has been studied recently for Al(100) where the resonances are located far away from the projected band gap.[15] This results in a strong coupling to the continuum of projected bulk bands and leads to excitation trapping, a phenomenon that is not observed for Ag(111).

As shown in Fig. 1(c), the probability densities of image-potential resonances are confined by the image-potential only on the vacuum side, while they infinitely penetrate into the bulk. The energies and probability densities shown in Fig. 1 for Ag(111) have been calculated by numerically solving the Schrödinger equation for an electron in an effective one-dimensional model potential.[8] On the Ag(111) and Cu(111) surface, the potential supports two bound solutions with energies within the projected band gap, which can be assigned to the Shockley surface state (SS) and the first image-potential state ($n = 1$). The amplitude of their wave functions decays exponentially into the bulk as depicted in Fig. 1(b). For energies above the upper edge of the surface-projected band gap there is no restriction of the wave function within the metal and a continuum of solutions can be obtained. Image-potential

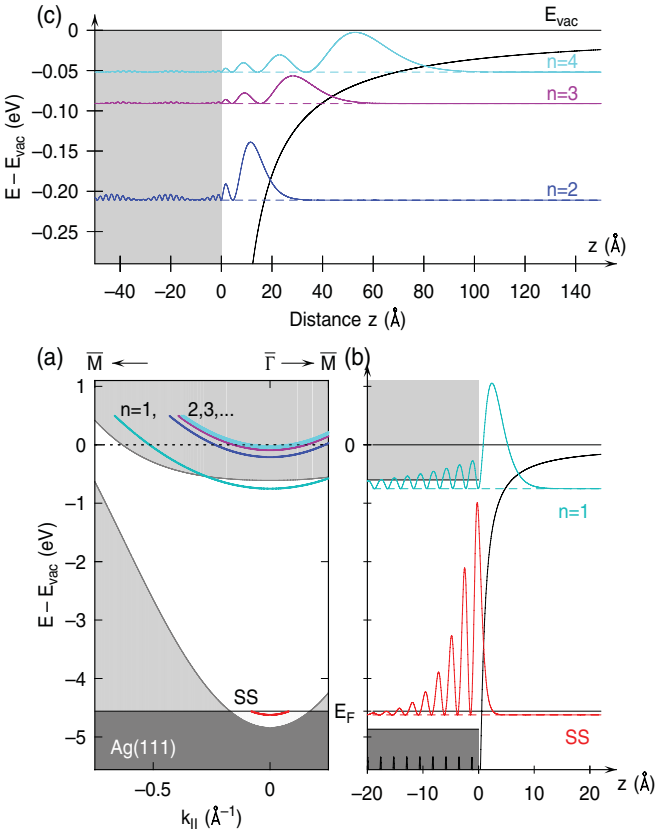

FIG. 1. (Color online) (a) Surface-projected band structure of Ag(111) close to the $\overline{\Gamma}$ point. The Shockley surface state (SS) close to the Fermi level E_F and the image-potential derived states close to the vacuum level E_{vac} are surface-specific electronic states with free-electron-like dispersion. Dark (light) shaded areas illustrate the occupied (unoccupied) surface-projected bulk bands,[7] while the white area resembles the surface-projected band gap. The energy scale is given with respect to the vacuum energy at the $\overline{\Gamma}$ point. (b) Calculated probability densities of the Shockley and the $n = 1$ image-potential states along the surface normal using a one-dimensional model potential[8] (solid black line). (c) Calculated probability density of the first three image-potential resonances $n = 2$–4.

resonances can be identified by a resonant enhancement of their probability density in front of the surface. Figure 1(c) depicts the calculated probability densities of the first three image-potential resonances $n = 2$–4 that form Bloch waves inside the bulk. The Bloch waves consist of a fast modulation with the periodicity of the crystal lattice superimposed with a slower modulation, which corresponds to the electron momentum in the bulk. This suggests that an electron, which is placed in front of the surface at an energy of one of these surface resonances, is transferred elastically into the bulk on an ultrafast timescale. Recent calculations using a wave packet propagation approach,[16] however, predicted rather long lifetimes of electrons in these image-potential resonances. In accordance with general arguments given in Ref. 4, the energies E_n and inelastic lifetimes τ_n of these resonances should follow hydrogenic scaling laws:

$$E_n = E_{vac} - \frac{0.85\ \text{eV}}{(n+a)^2}, \tag{1}$$

$$\tau_n \propto (n+a)^3 \tag{2}$$

with quantum number n. a is the quantum defect, which is related to the phase shift of the wave function compared to a pure hydrogen-like wave function. The identical scaling applies for the well studied image-potential states on Cu(100),[17,18] where the whole Rydberg series is located in the center of the surface-projected band gap. In order to experimentally determine energies, inelastic lifetimes as well as pure dephasing times of these closely lying resonances, we have used a combination of 2PPE and quantum-beat spectroscopy. This technique has already been successfully applied for the study of the image-potential states on Cu(100),[17,19,20] and it turns out that it is also well suited for image-potential resonances. Our experiment achieves a sufficiently high resolution in order to extend the previous experiments on the $n = 1$ state and the $n = 2$ resonance to resonances with quantum numbers up to $n = 7$.

This paper is organized as follows: after a description of the experimental setup, we first discuss the experimental results. The latter section is divided into the assignment of the different electronic states and resonances with the help of the time-resolved 2PPE spectra, the determination of the lifetimes of the separately lying $n = 1$ state and $n = 2$ resonance by conventional time-resolved 2PPE, and the description of the quantum-beat spectroscopy for the investigation of the resonances with $n \geqslant 3$. The subsequent section describes the analysis of the quantum-beat data. We follow the approach already applied for the image-potential states on Cu(100) but describe the evaluation in more detail than in Refs. 17 and 19. The analysis consists of a simplified but illustrative description of the observed wave packet dynamics using scaled hydrogen wave functions as well as a quantitative evaluation of the quantum-beat data within the framework of the density-matrix formalism. In Sec. VI, we discuss the experimentally determined energies, inelastic lifetimes, and pure dephasing times for the Rydberg series of resonances and compare them with recent theoretical calculations.

II. EXPERIMENT

All presented data were obtained with a setup similar to the one described in Refs. 21–24. It consists of an ultrahigh vacuum (UHV) chamber with a base pressure of 4×10^{-11} mbar, which is built out of μ-metal in order to suppress magnetic fields at the sample position. The output of a Ti:Sapphire oscillator operating at a repetition rate of 82 MHz was used as laser source. The laser was tuned to a central wavelength in the near infrared (IR) $\lambda_{IR} = 800$ nm (photon energy is $\hbar\omega_{IR} = 1.55$ eV, bandwidth (FWHW) is $\Delta\hbar\omega_{IR} = 47$ meV). The laser output was split into two parts. One part was frequency tripled by subsequent second-harmonic and sum-frequency generation providing photons with an energy of $\hbar\omega_{UV} = 4.68$ eV ($\lambda_{UV} = 265$ nm) and a bandwidth of $\Delta\hbar\omega_{UV} = 53$ meV, while the second part is guided over a motor-driven delay stage with a resolution better than 1 fs. Second-order dispersion of the laser pulses has been corrected for the near-IR and UV pulses separately by pairs of Brewster prisms made out of SF10 and fused silica, respectively. Both laser beams were aligned collinearly using a dichroitic mirror and were focused by a spherical Al mirror ($f = 50$ cm) into a spot with a diameter of about 100 μm onto the sample.

The laser pulse durations on the Ag sample were typically $\tau_{IR} = 45$ fs and $\tau_{UV} = 69$ fs.

Photoelectrons were detected with a hemispherical electron energy analyzer equipped with a five-channeltron-array detector. The energy resolution of the analyzer was $\Delta E_{Det} = 26$ meV with an acceptance angle of 1.4°. All 2PPE spectra have been recorded in normal emission geometry where the sample surface has been aligned perpendicular to the symmetry axis of the analyzer lens system. All energies are given with respect to the vacuum level E_{vac}, which is the natural reference level for image-potential states. Initially, the electron spectra are recorded relative to the Fermi level E_F. The spectral position of E_{vac} can be determined with high precision by the convergence of the Rydberg series with n [see Eq. (1)] if a sufficient number of states is measured.

The Ag(111) sample was prepared by repeated Ar^+ ion sputtering (20 minutes at $T_{Sample} = 370$ K with an energy of $E_{kin} = 700$ eV and an ion current of $I_{Sputter} = 3$ μA) and subsequent annealing cycles (5 minutes at $T_{Sample} = 770$ K). The sample cleanliness was checked by x-ray photoelectron spectroscopy (XPS) of the Ag-3d and C-1s signals and the long-ranged order by low-energy electron diffraction (LEED). Moreover, the absolute intensity at the low-energy cutoff of the 2PPE spectra, which depends on the work function Φ of the sample as well as the 2PPE signal of the first ($n = 1$) image-potential state are very sensitive probes for the quality of the surface. Therefore the 2PPE spectra themselves have been used as a monitor of the surface quality of the sample during the measurements. For all 2PPE measurements, the Ag(111) sample was cooled down to 83 K by liquid nitrogen, which increases considerably the signal-to-noise ratio of the 2PPE signal and reduces phononic contributions to the decay processes.

III. RESULTS

A. 2PPE spectra

The excitation scheme used in the present 2PPE study is shown in Fig. 2(a). The frequency-tripled UV pulses excite electrons from occupied states below E_F and populate the image-potential states near E_{vac}. The excitation can either occur from Ag bulk states of the sp band near the surface or from the Shockley surface state as indicated in the excitation scheme by long blue arrows. The transient population of the image-potential states is probed by photoemission using the fundamental laser pulses in the near IR. Energy-resolved 2PPE spectra for various temporal delays Δt between pump and probe pulses are shown in Fig. 2(b). For temporal overlapping laser pulses ($\Delta t = 0$), four distinct peaks from different 2PPE processes emerge in the spectrum. The largest peak at the lowest energy of $E - E_{vac} \approx -750$ meV arises from photoemission of the first ($n = 1$) image-potential state. The peak at a slightly higher energy of $E - E_{vac} \approx -460$ eV can be assigned to an excitation between Ag-bulk bands due to a direct nonresonant two-photon transition from the lower to the upper sp band.[25,26] At an energy of $E - E_{vac} \approx -210$ meV, the first image-potential resonance $n = 2$ can be observed as a clearly separated peak in the spectrum. The fourth peak on the high-energy side of the spectrum at $E - E_{vac} \approx -60$ meV is dominated at zero delay by a direct nonresonant two-photon

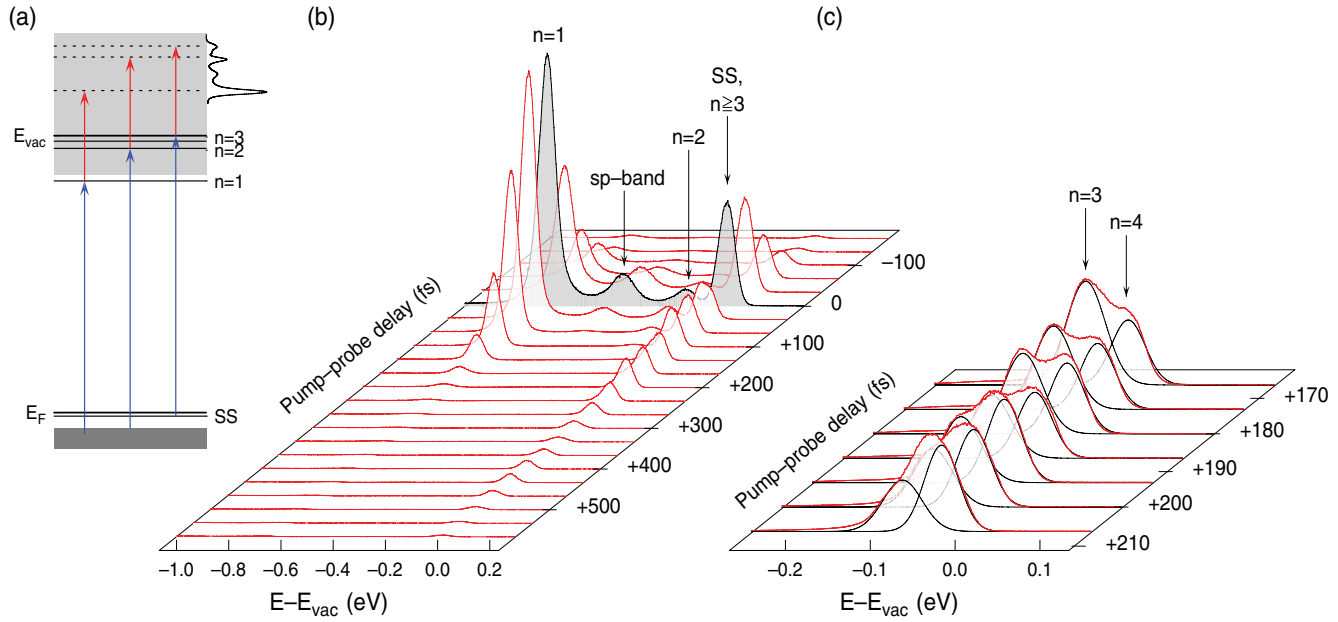

FIG. 2. (Color online) (a) Excitation scheme of the 2PPE experiment. UV photons (long blue arrows) excite electrons from below the Fermi level E_F into image-potential derived states near the vacuum level. The transient population of the image states is probed by laser pulses in the near IR (short red arrows). A high 2PPE yield for the higher lying image-potential resonances can be achieved by resonant excitation from the Shockley state (right arrows). (b) 2PPE spectra of Ag(111) for various pump-probe delays. At zero delay, the spectrum (grey shaded) consists of four clearly distinguishable peaks. The spectra for different delays reveal the electron dynamics in the respective states (see text for details). (c) 2PPE spectra close to E_{vac} and for larger pump-probe delay together with their deconvolution into two Gaussian lines (thin black lines), which represent the image-potential resonances $n = 3,4$.

transition from the occupied Shockley surface state (SS) to the detected final state. Please note that the energy scale given in Fig. 2 is misleading for the nonresonant two-photon excitations. In fact, the Shockley surface state is located close to the Fermi level E_F [see Fig. 2(a)] at $E - E_F = -0.063$ eV.[27]

We first discuss the decay dynamics of the different signals qualitatively, using the 2PPE spectra in Figs. 2(b) and 2(c) for different pump-probe delays in order to substantiate the assignment made above. For negative pump-probe delays Δt, the near-IR pulse arrives at the sample before any UV excitation can occur, while for positive Δt, the near IR pulses probe the population of intermediate states that has been generated by the UV photons. The 2PPE signal of the $n = 1$ image-potential state as well as for the $n = 2$ image-potential resonance decays rapidly toward positive Δt with comparable time constants. The fastest transient in the spectrum, however, is related to the *sp*-band transition, which is, as well as the excitation from the Shockley state, a nonresonant 2PPE process. Due to a missing transient population of an intermediate state, these two signals resemble the cross-correlation of the two laser pulses. For pump-probe delays exceeding the cross correlation, a further peak appears close to the spectral position of the Shockley state and close to E_{vac} and which can easily be detected up to $\Delta t = +550$ fs. This long-living peak is composed of several components as can be seen more clearly in Fig. 2(c), which is a blowup of Fig. 2(b) for energies around E_{vac} and pump-probe delays between $\Delta t = +170$ and $+210$ fs. The signal in this region originates from photoemission of image-potential resonances with quantum numbers $n \geqslant 3$. Around $\Delta t = +190$ fs, the image-potential resonances $n = 3$ and 4 can be resolved separately in the spectra. A deconvolution of the signal into two Gaussian contributions shows that the population of the $n = 3$ decays faster than that of the $n = 4$. With further increasing pump-probe delay the maximum of the 2PPE signal shifts continuously toward E_{vac} due to contributions of image-potential resonances with higher quantum numbers that cannot be entirely resolved.

The 2PPE signal of the image-potential resonances with $n \geqslant 3$ is significantly enhanced compared to the $n = 2$ signal due to the nearly resonant excitation from the Shockley state at a pump photon energy of 4.68 eV. This overcompensates a decreasing spatial overlap between the initial state and the intermediate image-potential state as well as between the intermediate state and the final, free continuum state with increasing quantum number. For the image-potential states on Cu(100), the dipole matrix elements for both transitions have been found to scale as $\propto (n + a)^{3/2}$, which reflects the hydrogen-like character of their wave functions.[17,28] The resonant excitation in the present experiment results in a less pronounced decrease with n and in a higher signal-to-noise ratio of the 2PPE signal for high n compared to Cu(100)[17,29] although the count rate of the $n = 1$ state is comparable on Cu(100) and Ag(111). The resonant excitation is, however, no prerequisite for the observation of the higher image-potential resonances.

B. Decay of isolated peaks

In order to analyze the decay dynamics of the excited electrons in detail, pump-probe traces have been recorded by variation of the pump-probe delay for different fixed kinetic energies. These transients correspond to cuts along the delay axis in Figs. 2(b) and 2(c) at the respective energies. Such pump-probe traces can be assigned to the decay dynamics of a single intermediate state only for the spectrally separated 2PPE signals of the $n = 1$ state and the $n = 2$ resonance. As shown in Fig. 3, the transients for these two states show a simple exponential decay for positive delays. The shorter lifetime of the $n = 2$ resonance compared to the $n = 1$ state is clearly visible and is in accordance with earlier experiments.[10] This is in contrast to the image-potential states on Cu(100) where the lifetime of the $n = 2$ state is three times larger compared to the $n = 1$ state. It reflects the fact that the $n = 2$ resonance on Ag(111) has an additional decay channel due to resonant one-electron transfer into the bulk. The lifetimes of the $n = 1$ state and the $n = 2$ resonance have been determined by a fit of the pump-probe traces using rate-equations under consideration of the finite temporal width of the laser pulses and an exponential population decay with a time-constant τ_n. The fits are shown as thin black lines in Fig. 3 and reveal inelastic lifetimes of $\tau_1 = 31.0 \pm 1.5$ fs and $\tau_2 = 23 \pm 2$ fs for the $n = 1$ state and the $n = 2$ resonance, respectively.

In particular, the $n = 1$ state shows an additional decay for negative pump-probe delays. For negative pump-probe delays, the intense near-IR pulse arrives at first and excites electrons around E_F. The excess energy of these electrons results in a broadening of the Fermi edge and electrons in the high-energetic tail of this nonthermalized distribution can now be photoemitted directly using one photon of the subsequent UV pulse. Within a time scale of about one hundred femtoseconds the electron distribution thermalizes, which leads to the observed decay. The dynamics of such hot electrons on (111)-oriented surfaces of different noble metals have been investigated extensively in Refs. 30–34 and will not be discussed further here.

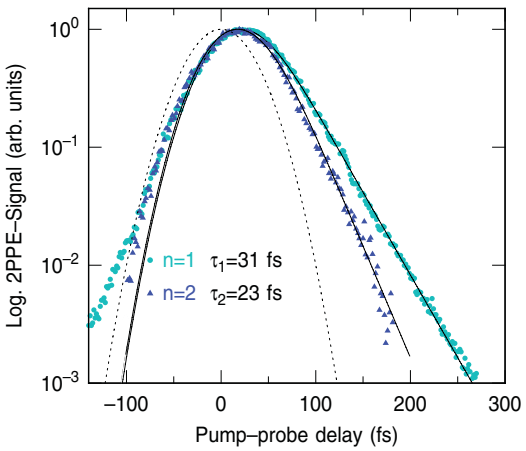

FIG. 3. (Color online) Semilogarithmic plot of the 2PPE intensity as a function of pump-probe delay at the energies of the first image-potential state ($n = 1$) and resonance ($n = 2$), respectively (data points). Lifetimes were obtained from fits using rate equations (solid lines). The cross correlation of the laser pulses is depicted as a dashed line for comparison.

C. Quantum-beat spectroscopy

The image-potential resonances with $n \geqslant 4$ cannot be fully resolved in the 2PPE spectra. The finite bandwidth of the pump pulse, however, makes it possible to coherently excite several adjacent image-potential resonances for $n \geqslant 3$ as illustrated in Fig. 4. This allows the application of quantum-beat spectroscopy for the determination of energies and lifetimes of these close-lying resonances.[17] Figure 4 additionally shows a typical 2PPE spectrum of Ag(111) at a pump-probe delay of about $\Delta t = 100$ fs. At this delay, the nonresonant photoemission of the Shockley state has already disappeared and the 2PPE signal of the higher image-potential resonances becomes visible.

Time-resolved 2PPE data have been recorded for different energies close to E_{vac} as indicated by arrows in the 2PPE spectrum of Fig. 4. These pump-probe traces are shown in Fig. 5 for pump-probe delays up to 3 ps. In contrast to the simple exponential decay of $n = 1,2$, all other transients show pronounced oscillations superimposed on an overall decay. The time scale of the decay reaches the ps range close to E_{vac}. This shows that the image-potential resonances with high quantum numbers have rather long lifetimes in spite of the presence of resonant electron transfer into the bulk. Accompanied by the steadily increasing decay time, the oscillations become more pronounced and their frequency decreases with decreasing binding energies. In particular, this can be seen by comparing the transients taken for energies between $E - E_{\mathrm{vac}} = -70$ and -19 meV. In addition, the oscillation frequency decreases with increasing pump-probe delay. At $E - E_{\mathrm{vac}} = -54$ meV, for example, the oscillation of the 2PPE signal has a higher frequency up to a pump-probe delay of ~700 fs compared to larger delays where the frequency steadily decreases until all signals have decayed.

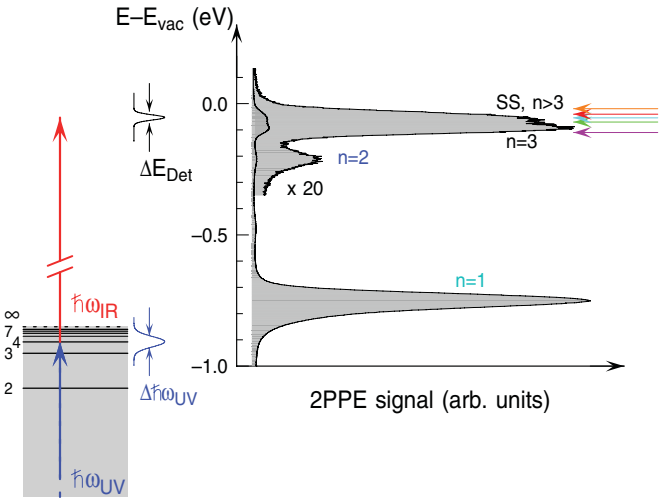

FIG. 4. (Color online) (Left) Sketch of the 2PPE excitation and photoemission of image-potential resonances with $n \geqslant 3$. The finite band width $\Delta\hbar\omega_{\mathrm{UV}}$ of the excitation pulses leads to a coherent excitation of several neighboring image-potential resonances (black lines). The photoemission with the near-IR pulse probes the temporal evolution of the superposition of the excited resonances with a spectral resolution that is mainly determined by the resolution of the electron analyzer ΔE_{Det}. (Right) 2PPE spectrum for a pump-probe delay of about $\Delta t = +100$ fs where the nonresonant contribution from the Shockley surface state has already disappeared. The arrows in the spectrum indicate the energies at which the time-resolved 2PPE data shown in Fig. 5 have been recorded.

The oscillation of the 2PPE signal originates from the interference between the coherently excited image-potential resonances. The photoemission intensity $I(t)$ is proportional to the probability density of the excited state. In the case of two coherently excited states $\Psi_n(t) = e^{i\omega_n t}|n\rangle$ and $\Psi_{n+1}(t) = e^{i\omega_{n+1} t}|n+1\rangle$, with $\omega_n = E_n/\hbar$, it has the following time dependence:

$$I(t) \propto |a_n(t)\Psi_n(t) + a_{n+1}(t)\Psi_{n+1}(t)|^2$$
$$\propto a_n^2(t) + a_{n+1}^2(t) + 2a_n(t)a_{n+1}(t)\cos(\omega_{n,n+1}t).$$

Thus the pump-probe trace of the 2PPE intensity is modulated by a beat frequency $\nu_{n,n+1} = \omega_{n,n+1}/2\pi = |E_n - E_{n+1}|/h$, which is proportional to the energy separation of the coherently excited states. The decrease of the beat frequency with decreasing binding energy and with increasing pump-probe delay observed in the experiment can therefore be explained by a growing contribution of states with a smaller energy separation. These low-frequency modulations are detected in the 2PPE experiment in the time domain and give access to energy spacings that by far exceed the energy resolution of the electron detector ΔE_{Det} (compare Fig. 4).

IV. ANALYSIS OF QUANTUM-BEAT DATA

A. Wave packet description

Prior to a quantitative analysis we first discuss the spatial and temporal evolution of the coherently excited electrons in terms of wave packets in order to illustrate the origin of the different decay dynamics. For this description, we make use of the formal analogy between the one-dimensional Schrödinger equation for an electron in the classical image-potential $V(z) = -e/4z$ and the radial Schrödinger equation of an electron in the Coulomb-potential $V(r) = -e/r$ with angular momentum $\ell = 0$. Here, z is the distance perpendicular to the surface and r is the radial distance. Therefore the wave function of an electron in an idealized image-potential state corresponds to a scaled s-like radial hydrogen wave function $R_n^{\ell=0}(z/4)$ multiplied by z and expanded by a factor of four.

A coherent excitation of image-potential states with quantum numbers n creates a wave packet

$$\Psi_{\mathrm{WP}}(z,t) = \sum_n a_n(t) z R_n^{\ell=0}(z/4) e^{-i\omega_n t} \qquad (3)$$

in front of the surface. Inelastic decay of the excited population has been included by time-dependent amplitudes $a_n(t) = a_n e^{-t/2\tau_n}$. The loss of coherence due to pure dephasing of the wave packet is omitted here. Energies E_n, excitation probabilities a_n as well as the inelastic lifetimes have been taken from the quantitative analysis of the pump-probe traces as described below. A Gaussian weighted excitation distribution around the detected energy with a width of $\Delta E_{\mathrm{ex}} = 0.055$ meV imitates the bandwidth of the exciting laser pulse. For each of the pump-probe traces shown in Fig. 5, the respective wave packet was composed of image-potential states with quantum numbers $n = 3$–20. The resulting

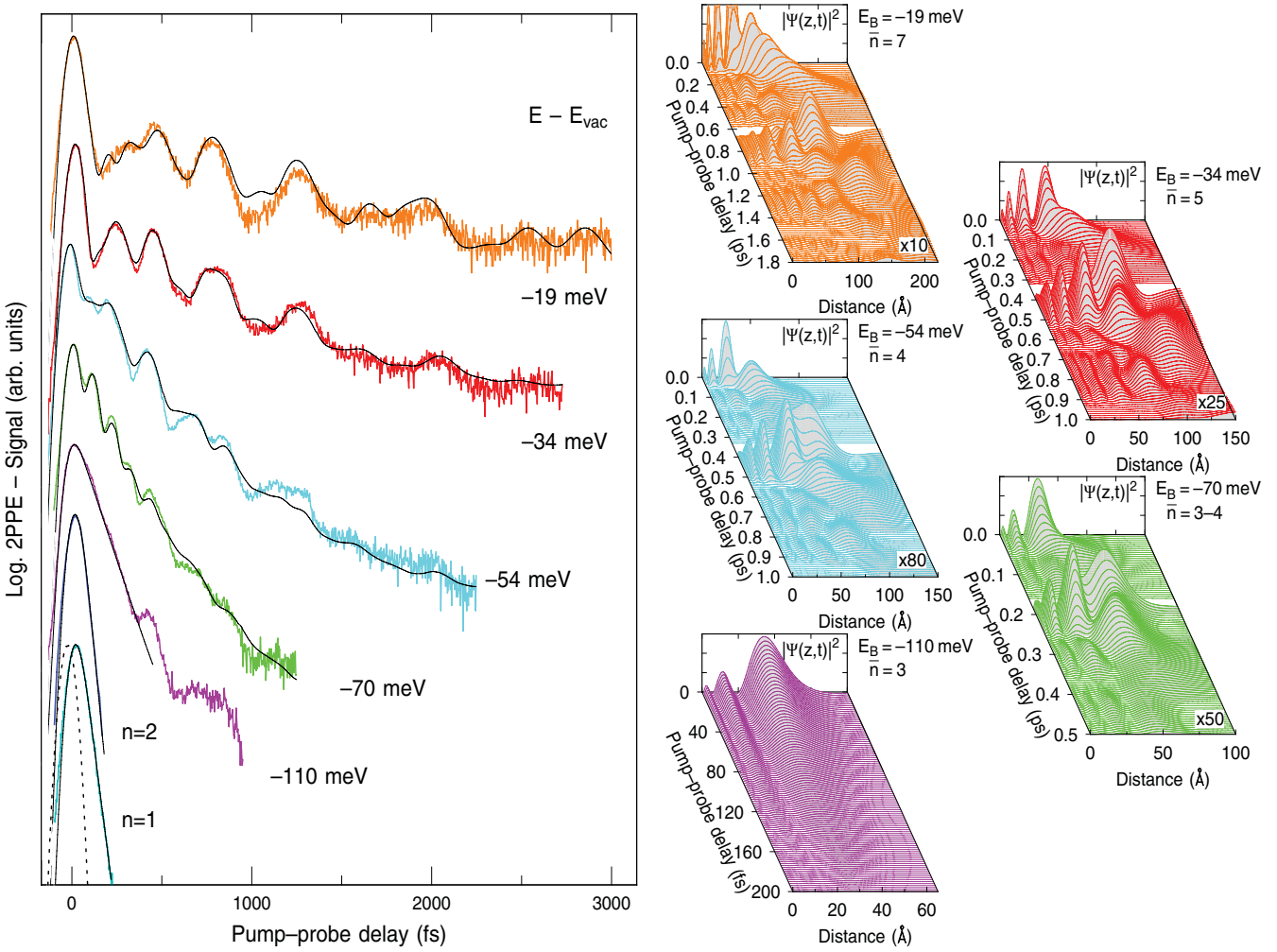

FIG. 5. (Color online) (Left) Semilogarithmic plot of the time-resolved 2PPE data for different energies of the intermediate state (colored lines) and respective fits using the density matrix formalism (thin black lines). The pump-probe traces for $n = 1,2$, already shown in Fig. 3, have been plotted again for comparison. All other transients reveal beating patterns due to the coherent excitation of image-potential resonances with different quantum numbers. (Right) Calculated spatial and temporal evolution of the probability density of wave packets composed of a coherent superposition of hydrogenic states. For these simulations the experimentally determined energies, lifetimes, and transition matrix elements of the image-potential resonances have been used (see text for details). The 2PPE intensity is proportional to the probability density of the electron close to the surface ($z = 0$). Please note the different scalings of the axes.

probability density $|\Psi_{\mathrm{WP}}(z,t)|^2$ in front of the surface is plotted in Fig. 5 using a linear scale. Due to the large range of the decay dynamics, a different scaling of the spatial and temporal axes has been used for each simulation. In order to take account of the decay, the scale has been changed for large delays by a factor as indicated in the respective figures. The 2PPE intensity can be related to the probability density of the electron close to the surface ($z \approx 0$) where the gradient of the image-potential is large enough to provide the required momentum for the photoemission by the probe pulse. Within this picture, it is assumed that an excited electron within the classical image-potential is located only in front of the surface. The coupling to the metal due to inelastic decay as well as due to elastic transfer into the bulk in the case of resonances is effectively described by a single decay rate of the probability density in front of the surface.

A comparison between the experimental pump-probe traces and the temporal evolution of the simulated wave packets shows that even this simplified description using solutions for the pure classical image-potential reproduces most of the observed dynamics. For $E - E_{\mathrm{vac}} = -110$ meV, where the $n = 3$ resonance is detected almost exclusively, both, the 2PPE signal as well as the simulated probability density, decay exponentially for delays up to 200 fs. For energies closer to E_{vac}, the oscillations become more pronounced. In order to reproduce these quantum-beat patterns, a growing number of image-potential states with higher quantum number and increasing inelastic lifetime have to be included in the simulated wave packets. The pump-probe trace for $E - E_{\mathrm{vac}} = -54$ meV, for example, is described by a wave packet of image-potential states with a mean quantum number $\bar{n} = 7$. The maxima of the 2PPE intensity at 0, 0.2, 0.45, 0.8, and 1.25 ps can be well reproduced by the wave packet motion. The decreasing oscillation frequency with decreasing energy separation from E_{vac} clearly correlates with the growing mean quantum number. This goes along with a decreasing energy

separation of the adjacent states. At the same time, the spatial extent of the wave packet motion increases. With growing mean quantum number, the wave packet dynamics resembles more and more the classical motion of an electron that bounces back and forth in front of the surface.

B. Modeling of the 2PPE process

A full description of the coherent optical excitation, the temporal evolution of the induced optical polarizations and populations with consideration of elastic and inelastic decay, and the subsequent photoemission can be achieved by the application of a density matrix formalism.[13,17,18,28,35,36] Here, we follow the notation of Ref. 28. Within this formalism, the electronic structure of the surface is represented by a density matrix $\hat{\rho}$ with diagonal and off-diagonal elements that describe the populations and coherences of an N-level system, respectively. The coherent dynamics is then described by the Liouville-von Neumann equation,

$$i\hbar\frac{\partial\hat{\rho}}{\partial t} = [\hat{H},\hat{\rho}] + \frac{\partial\hat{\rho}_D}{\partial t}, \tag{4}$$

where $\hat{H} = \hat{H}_0 + \hat{H}_L$ is the full Hamiltonian that consists of the Hamiltonian of the unperturbed system $\hat{H}_0$ with eigenfunctions ψ_α and energies E_α ($\alpha = 1,\ldots,N$), and the Hamiltonian $\hat{H}_L$, which describes the interaction with the laser fields. The latter is typically treated in a semiclassical description within the dipole approximation, where it is given by $\hat{H}_L = -\hat{\mu}\cdot\boldsymbol{\mathcal{E}}(t)$ with the dipole operator $\hat{\mu} = -e\boldsymbol{r}$ and the classical electric field $\boldsymbol{\mathcal{E}}(t)$. For image-potential states with their free-electron-like character parallel to the surface, only the component of the dipole operator perpendicular to the surface is relevant and therefore $\hat{H}_L = -ez\mathcal{E}_z(t)$. The coupling to the environment is described phenomenologically by a dissipation matrix $\hat{\rho}_D$. For simple exponential decay it has the form $\hat{\rho}_{D,\alpha\beta} = -\Gamma_{\alpha\beta}\hat{\rho}_{\alpha\beta}$, where the $\Gamma_{\alpha\beta}$ are the elements of a damping matrix. Its diagonal elements are given by the inelastic decay rates $\Gamma_{\alpha\alpha} = \hbar/T_{1,\alpha} =: \tau_\alpha$ is the inelastic lifetime of state α. Sometimes, τ_α is also denoted as energy relaxation time. Typically, the inelastic lifetimes of the initial and final states are assumed to be infinite. The off-diagonal rates $\Gamma_{\alpha\beta}$ describe the decay or dephasing of the polarization between different states. It is convenient to separate them into contributions of each state by $\Gamma_{\alpha\beta} = \Gamma_\alpha + \Gamma_\beta$. Dephasing of the polarization can occur due to inelastic decay as well as due to elastic scattering. Therefore, the dephasing rate is further separated into $\Gamma_\alpha = \hbar/(2\tau_\alpha) + \hbar/T^*_{2,\alpha}$, where $T^*_{2,\alpha}$ is often called "pure" dephasing time. Since the final state in 2PPE describes an electron that leaves the surface and is detected in the electron spectrometer, the pure dephasing time of that state can be also assumed to be infinite. Note that $2\tau_\alpha$ enters into Γ_α because the polarization is proportional to the amplitude of a harmonic oscillator, whereas the energy is proportional to the square of the amplitude. Therefore the inelastic contribution to the decay rate of the polarization (amplitude) is only half of the energy relaxation rate in the case of exponential decay.

The free parameters of a description within the density matrix formalism are the dipole matrix elements $\langle\psi_\alpha|\hat{\mu}|\psi_\beta\rangle$, the energies E_α, the inelastic lifetimes τ_α as well as the pure dephasing times $T^*_{2,\alpha}$. However, only certain 2PPE schemes as quantum-beat spectroscopy,[17,19–22,37] interferometric 2PPE,[38–41] line-width measurements,[42] or the recently developed method of optical induced electrical currents[43] are capable of accessing pure dephasing times that provide information about quasi-elastic scattering processes.[44] In quantum-beat spectroscopy, the pure dephasing is responsible for the decay of the oscillations of the pump-probe traces, whereas the inelastic lifetime describes the overall decay.

For a realistic description of even the most relevant part of the electronic surface structure, the size of the density matrix and therefore the number of free parameters can be rather large. This is in particular the case if the initial or intermediate states form a continuum that might be represented by many close-lying states. For the Ag(111) surface, the most relevant initial state is the Shockley surface state. The image-potential resonances can be described effectively by a Rydberg series of discrete states where the coupling to the continuum of projected bulk states is included in the empirical inelastic decay time. The continuum of final states in the vacuum can be considered by an incoherent sum of the 2PPE signal for a series of final states within the bandwidth of the electron detector.

Even with these restrictions, a fitting of the experimental pump-probe traces within the full density matrix formalism is very time consuming, since for each pump-probe delay, the full set of differential equations has to be solved for a time-interval that increases with pump-probe delay. On the other hand, the energies and lifetimes of the image-potential states or resonances affect the pump-probe traces almost only for pump-probe delays that are larger than the cross correlation of pump and probe pulses. For these pump-probe delays, the 2PPE signal is effectively a direct image of the population of the image-potential resonances. This renders possible the application of some simplifications,[19] which drastically reduce the computational effort: (1) the excitation by the pump pulse and the photoemission by the probe pulse are decoupled by approximating the photoemission by a weighted projection of the population of the coherently excited states into the continuum. The weighting corresponds to the emission probability and is described by a power law $\propto(n+a)^{-3}$. (2) The energies of image-potential states or resonances are parameterized by the Rydberg formula [see Eq. (1)], with the quantum defect a as a free parameter for the energy differences. (3) The dipole matrix elements for the excitation are scaled using a power law $\propto (n+a)^{-3/2}$ that results in an identical power law for excitation and emission probability. (4) Each pump-probe trace is fitted using inelastic lifetimes and pure dephasing times of the three contributing resonances with the lowest quantum number as free parameters. Lifetimes and pure dephasing times of the subsequent higher resonances with n up to 13 are scaled by a power law $\propto(n+a)^3$ according to their Rydberg-like character. Within this description, there is no distinction between image-potential states and resonances. The inelastic lifetime describes effectively the loss of population in the corresponding intermediate state. This loss results from inelastic decay and, in the case of resonances, also from elastic transfer into the bulk where the electron can no longer be detected by photoemission.

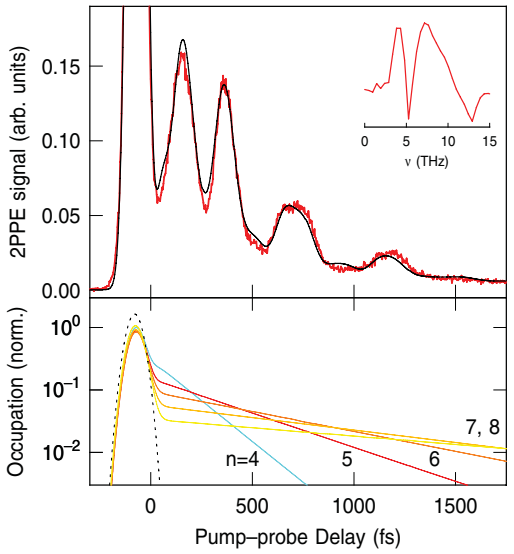

FIG. 6. (Color online) (Top) Pump-probe trace recorded at $E - E_{\mathrm{vac}} = -34$ meV together with the results of the fit using the density matrix formalism (black line). The individual states that contribute to the beating pattern and their inelastic lifetimes can be extracted from this simulation. The inset shows the Fourier transform of the experimental spectrum after subtraction of a smooth exponential background. The signal is composed of a coherent superposition of neighboring image-potential resonances for positive delays and an additional component due to nonresonant 2PPE around zero delay. The lower part depicts the relative occupations of the resonances (solid line) and the nonresonant direct 2PPE contribution (dashed line).

The experimental data were fitted iteratively until all pump-probe traces could be described by one set of parameters consisting of inelastic lifetimes τ_n, pure dephasing times $T_{2,n}^*$, and the quantum defect a. The fits are shown as thin black lines in Fig. 5. Moreover, Fig. 6 depicts the pump-probe trace taken at $E - E_{\mathrm{vac}} = -34$ meV together with the results of the fit. The data have been normalized with respect to the maximal signal. The large 2PPE signal around zero delay has been cut in order to highlight the quantum-beats on a linear intensity scale. The experimental data are reproduced almost perfectly by the fit. Slight deviations in this exemplary spectrum result from the demand that all pump-probe traces should be described by one set of fitting parameters. The pump-probe trace shown in Fig. 6 consists of contributions from the image-potential resonances $n = 4$–8 and an additional contribution from nonresonant photoemission of the occupied Shockley state, which resembles the cross correlation of the laser pulses (see also Fig. 2). The relative contributions of the adjacent resonances to the coherent dynamics are shown in a semilogarithmic plot in the lower panel of Fig. 6. The population decays exponentially with inelastic lifetimes τ_n that strongly increase with the quantum number n. The main contribution to the signal for a pump-probe delay up to 500 fs originates from the resonances $n = 4$ and 5. The comparatively large energy separation between these two states results in a relatively high oscillation frequency. At about 600 fs, the beating pattern changes and the frequency decreases, which indicates a smaller energy separation between the contributing states. This originates from the contribution of the higher-lying states $n = 5$–7.

The inset of Fig. 6 depicts a Fourier transform of the experimental data after subtraction of an exponential decay. The beating frequencies $\omega_{n,m}$ and therefore the energy separation $E_n - E_m$ between the contributing states can in principle be also extracted from this Fourier transform. Its resolution, however, strongly depends on the number of available experimental data points. Especially for low frequencies, the lacking resolution in the frequency spectrum is a drawback of this procedure compared to the data evaluation in the time domain.

C. Collected results

The time-resolved 2PPE data of the states $n = 1,2,3$ and the quantum-beat spectroscopy of the states $n \geqslant 3$ allow us to determine the binding energies and lifetimes of the whole Rydberg series up to $n = 7$. Values for resonances with higher quantum numbers $n \geqslant 8$ could not be extracted as independent parameters from the pump-probe traces, because on one hand, the signal-to-noise ratio of the data decreases very close to E_{vac} and on the other hand, more and more states are coherently excited and contribute to the signal. In this energy regime, it would be advantageous to perform the experiment with longer, more narrow-band laser pulses. Table I summarizes all experimentally determined energies and lifetimes for the $n = 1$ image-potential state and the resonances $n = 2$–7. In addition, the table contains the experimental dephasing times for the resonances $n = 3$–7 and theoretical values for energies and lifetimes that will be discussed below.

V. DISCUSSION

A. Energies

Before we compare the experimental energies with theoretical predictions, it is important to emphasize that the resolution of the series of resonances up to $n = 7$ enables us to determine the position of the vacuum level E_{vac} with high accuracy and to give precise values of the energies E_n with respect to E_{vac}.

TABLE I. Experimental (exp.) and theoretical (theor.) energies $E_n - E_{\mathrm{vac}}$, lifetimes τ_n, and pure dephasing times $T_{2,n}^*$ of the first seven image-potential states ($n = 1$) and resonances ($n = 2$–7) of Ag(111).

	$E_n - E_{\mathrm{vac}}$ (meV)		τ_n (fs)		$T_{2,n}^*$ (fs)
n	exp.	theor.[a]	exp.	theor.	exp.
1	-756 ± 3	-764.2	31.0 ± 1.5	18.3[b]	-
2	-212 ± 10	-212.6	23 ± 2	17.3[c]	-
3	-91 ± 2	-94.5	65 ± 5	52[c],54[d]	300 ± 50
4	-51 ± 1	-53.1	166 ± 20	122[c],116[d]	470 ± 100
5	-33 ± 1	-34.0	393 ± 40	246[c],227[d]	680 ± 150
6	-23 ± 1	-23.6	683 ± 80	397[c],375[d]	1100 ± 200
7	-17 ± 1	-17.4	1088 ± 140	588[d]	1800 ± 400

[a]Two-band model, $\phi_c = 0.89\pi$ ($a = 0.055$) for $n = 1$ and $\phi_c = \pi$ ($a = 0$) for $n \geqslant 2$.
[b]Reference 45.
[c]Reference 16 based on the model potential of Ref. 8.
[d]Our own calculations using the same model potential.

The best and most reliable results are obtained by retaining the quantum defect a as a free parameter in the fits of the quantum-beat pump-probe traces as outlined above. The best fit yields a small quantum defect of $a = 0.064(5)$. With the use of Eq. (1), this defines very precisely the position of E_{vac} with respect to that of the $n = 3$ resonance. The kinetic energy of the photoelectron originating from this resonance can be determined reliably in the raw 2PPE spectra (compare Fig. 2). This makes it possible to determine also the energies of the $n = 1$ state and the $n = 2$ resonance precisely with respect to E_{vac} because their positions are measured very accurately relative to the position of $n = 3$. The uncertainty of these energies is thus limited only by the accuracy with which the kinetic energy of the corresponding peaks can be determined, e.g., ± 3 meV in case of the $n = 1$ state. In Fig. 7, the experimental energy positions are shown in comparison with the basic Rydberg formula $E_n = E_{\mathrm{vac}} - 0.85\ \mathrm{eV}/n^2$. The error of all experimental data points in this plot is smaller than the size of the circles.

The binding energy of 0.756 eV of the $n = 1$ gap state corresponds to a quantum defect of $a = 0.060$ in Eq. (1). In the multiple scattering model of Echenique and Pendry,[4] the quantum defect results from a phase shift ϕ_c of an electron reflected at the surface that deviates from π [$a = \frac{1}{2}(1 - \phi_c/\pi)$]. This phase shift is easy to calculate using a two-band model to describe the electronic structure of Ag(111).[46,47] With the parameters for Ag(111) given in Ref. 8, one obtains $\phi_c = 0.89\pi$, $a = 0.55$, and $E_{n=1} = 0.764$ eV. This suggests that such an idealized model of Ag(111) indeed provides an adequate description of the image-potential state $n = 1$. The same is true for the series of image-potential resonances. At the top of the gap and for higher energies, the phase shift ϕ_c reaches π in the two-band model, resulting in a vanishing quantum defect. The measured energy of the $n = 2$ resonance exactly corresponds to $a = 0$. Also the quantum defect resulting from the best fit of the quantum-beat data ($a = 0.064$) is close enough to zero such that the whole series of resonances can be satisfactorily described without the introduction of a quantum defect (c.f. Fig. 7).

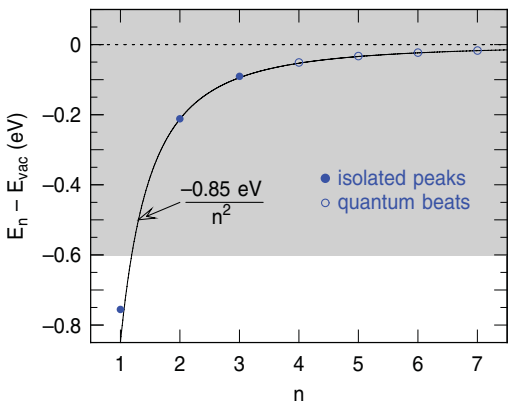

FIG. 7. (Color online) Energies $E - E_{\mathrm{vac}}$ of image-potential derived states on Ag(111) (data points). The projected bulk bands are depicted by the gray shading. The solid line shows a power law $\propto n^{-2}$ according to Eq. (1) with $a = 0$.

B. Lifetimes

The lifetime of the $n = 1$ state ($\tau_1 = 31.0 \pm 1.5$ fs) is in good agreement with the results determined earlier by Harris and coworkers ($\tau_1 = 32 \pm 10$ fs)[10] but clearly longer than the value of 20 fs deduced from the first time-resolved 2PPE experiment by Schoenlein *et al.*[9] As compared to Cu surfaces, the inelastic lifetimes of the first image-potential state on both the (100) and the (111) surface of Ag are significantly longer [$\tau_1 \geqslant 20$ fs in the case of Cu(111)].[14,18,32] This is surprising since the screening of the d electrons in Ag reduces the energy of the surface plasmon below the energy of the image-potential states,[48,49] which opens a further inelastic decay channel in addition to electron-hole-pair excitation. García-Lekue *et al.*[45,50] however, showed that although the screening of the d electrons enhances the imaginary part of the self-energy near the surface, its nonlocal character effectively leads to an increase of the inelastic lifetime. The calculated lifetime of the $n = 1$ state on Ag(100)[50] is in excellent agreement with the experiment.[18] For the $n = 1$ state on Ag(111), however, theory apparently underestimates the inelastic lifetime by about 60% ($\tau_1 = 18.3$ fs).[45]

Previous experiments have provided an upper limit of 20 fs for the lifetime of the image potential resonance $n = 2$.[9,10] Our result of $\tau_2 = 23 \pm 2$ fs lies only slightly above this limit. The shorter lifetime of the $n = 2$ resonance compared to the $n = 1$ gap state reflects the fact that resonant electron transfer into the bulk constitutes an efficient additional decay channel for image-potential resonances. On Cu(111), it could be shown that the decay characteristics of the corresponding $n = 1$ state change drastically if the quasistationary state is transformed into a resonance by shifting its energy above the band gap with the help of adsorbed Ar layers.[14] Obviously, the resonant transfer rate of the $n = 2$ resonance must exceed the general decrease of the inelastic decay rate due to electron-hole-pair excitation with quantum number in order to result in a higher total decay rate and therefore shorter lifetime as compared to the $n = 1$ state.

Borisov *et al.*[16] investigated the decay of the series of Ag(111) image-potential resonances using the one-dimensional potential of Chulkov *et al.*[8] This model potential has been constructed based on the well-known Ag band structure and an energy position of -0.77 eV for the first image-potential state, i.e., the value determined by Steinmann and coworkers,[51] which is in good agreement with the present result. In order to calculate the rate of elastic electron transfer into the bulk, Borisov *et al.* obtained wave functions $\psi(z,t)$ by solving the time-dependent Schrödinger equation for this model potential. The initial wave function $\psi(z,t = 0)$ describes a wave packet located on the vacuum side. The decay rate Γ_n is given by the Laplace transform of the survival amplitude $\langle \psi(z,t=0)|\psi(z,t)\rangle$.[16] An equivalent and nearly identical result can be obtained from the stationary solutions of the time-independent Schrödinger equation for the same model potential. Within the latter method, linewidths Γ_n are determined from peaks of the total probability density in front of the surface as a function of energy.[14,52] Corresponding lifetimes $\tau_n = \hbar/\Gamma_n$ from both calculations are collected in Table I.

Experiment and theory qualitatively agree insofar as they both show a strong increase of the lifetime with quantum

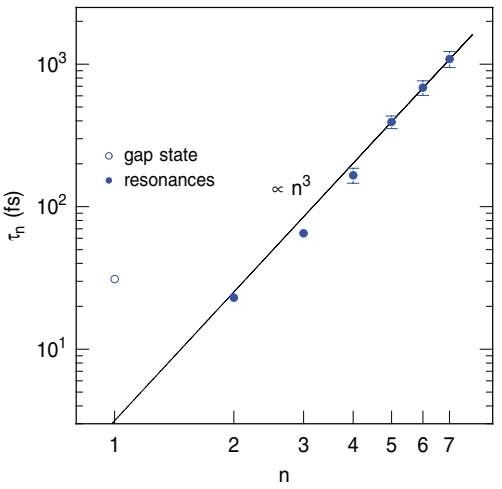

FIG. 8. (Color online) Experimentally determined inelastic lifetimes of image-potential states and resonances of Ag(111) (dots). The solid line indicates a dependence $\tau_n = 3.15\,\text{fs} \times n^3$.

number from $n = 2$ to 7. The dependence approximately follows the general scaling law $\tau_n \propto n^3$ (see Fig. 8). Echenique and Pendry have predicted this scaling law for the lifetime of image-potential states as well as for resonances.[4] After the experimental confirmation for the gap states of Cu(100)[17] and Ag(100),[18] our results represent the first experimental confirmation of this prediction for image-potential resonances. The n^3 scaling is also in excellent agreement with the wave packet calculations of Borisov *et al.*[16]

When we compare the extrapolation of the n^3 scaling to $n = 1$ with the measured decay time of the $n = 1$ state, we can obtain an estimate of the ratio between inelastic and elastic decay rate of the resonances. The extrapolated value for $n = 1$ is 3.15 fs, a factor of ten less than the measured lifetime of 31.5 fs. Under the assumption that also the inelastic decay follows the n^3 scaling, this suggests that roughly 10% of the measured decay rates of the resonances should be due to inelastic processes and 90% due to resonant electron transfer into the bulk. In Ref. 16, it has been argued that inelastic decay plays a minor role for the image-potential resonances because the many-body effects, which are responsible for the inelastic decay, become active only after the electron is already lost from the population of the quasistationary state at the surface. This has been deduced from the fact that the inclusion of an optical potential, which describes the many-body interactions in the bulk, has no effect on the calculated widths of the resonances.[16] In such a scenario, the estimate based on n^3 scaling would not be applicable and would even overestimate the importance of inelastic decay processes. However, also direct surface excitations may be very important for the inelastic decay. In case of the structurally similar Cu(111), e.g., decay into the Shockley surface state was shown to be a major decay channel.[53]

It is also interesting to compare the absolute values of the measured and calculated resonance lifetimes. For all the resonances, the experimental values exceed the theoretically predicted ones (c.f. Table I). The deviation is 30% for the $n = 2$ resonance. It gets larger with increasing n and amounts to a factor of two for $n = 7$. A deviation in this direction (underestimation of the lifetimes by theory) is surprising because the calculations do not include all possible decay processes but only consider resonant electron transfer. Although the inelastic electron-hole-pair decay is likely to contribute only to 10%, the inclusion of this and other processes such as interband decay[44,54,55] or electron-phonon scattering can only further increase the discrepancy between theory and experiment.

On the experimental side, an important question is, of course, to which extent the lifetimes measured by 2PPE reflect the inverse loss rate from the surface into the bulk. Due to the finite penetration depth of the light and the finite escape depth of the low-energy electrons, it is principally possible that the 2PPE experiment still detects electrons as they have already escaped into the bulk. The photoemission matrix element for the 1.5-eV probe photons, however, is appreciable only close to the surface, which renders the detection of the excited-state-population very surface sensitive.

On the theory side, a reason for the significant difference between experimental and theoretical lifetimes might have its origin in the model potential.[8] Many-body calculations based on similarly constructed potentials for other surfaces yield inelastic lifetimes of image-potential states that are in excellent agreement with experiment.[6,56,57] The potential, however, is less well tested for problems of resonant electron transfer. The reflection and transfer of the electron wave at the surface is probably more sensitive to specific details of the potential close to the surface compared to the spatial distribution of the probability density that governs the inelastic decay.

C. Dephasing times

The pure dephasing times, which could be determined from the analysis of the quantum-beat data for the image-potential resonances with quantum numbers $n \geqslant 3$ (see Table I), are significantly shorter compared to the image-potential states of Cu(100)[17,19,20] but still longer compared to the inelastic lifetimes. Pure dephasing can result from quasi-elastical electron scattering at steps, defects, and phonons.[44] The influence of defects has been systematically studied for the image-potential states on Cu(100) where it has been shown that CO molecules efficiently decrease the pure dephasing times but have almost no influence on the inelastic lifetimes.[20] Cu adatoms, on the other hand, mainly lead to a dramatic decrease of the inelastic lifetimes even for very low concentrations.[37,58] In the present work, we have not studied the influence of residual defects of our nominal clean Ag(111) surface on the observed pure dephasing times. The role of phonons, however, has been estimated by comparing our data taken at 83 K with measurements at room temperature. The latter have a higher background and a reduced signal-to-noise ratio but show no significant change of the pure dephasing times within the specified error bars and only a slight reduction of the inelastic lifetimes in the order of 10–30%. We therefore conclude that phonons do not significantly contribute to pure dephasing of the image-potential resonances and that the observed dephasing times are finally limited by the residual defect density of our sample. This is remarkable since the contribution of phonons is expected to scale with the large bulk penetration of the resonance wave functions. Even a weak electron-phonon coupling should therefore have a much stronger influence

on the dephasing of image-potential resonances compared to image-potential states within the projected band gap. This result, together with the scaling of energies and inelastic lifetimes, shows that the image-potential resonances behave very similar to quasistationary image-potential states with a certain finite bulk penetration.

VI. CONCLUSION

A combination of two-photon photoemission and quantum-beat spectroscopy has been applied to study the decay of electrons excited into image-potential resonances on a Ag(111) surface for quantum numbers up to $n = 7$. The hydrogen-like scaling of energy and lifetime with quantum number is in accordance with theoretical predictions and similar to image-potential states on Cu(100) where the whole series of states is located within the projected band gap. Although electrons excited into these resonances can decay by energy-conserving resonant electron transfer into the bulk, lifetimes of more than 1 ps could be observed. Surprisingly, the experimentally determined lifetimes are even longer than theoretically predicted. Our results show that the formation of a Rydberg series of hydrogen-like states with long lifetimes is not reliant on a gap in the projected band structure. Conclusions on the size and position of the band gap from the existence of long-living image-potential states[59] therefore have to be drawn with care. The observation of long lifetimes for electronic surface states that are resonant to bulk states has also important consequences for electron transfer across interfaces in general. It shows that energy alignment is a necessary but not a sufficient prerequisite for fast and efficient transfer.

ACKNOWLEDGMENTS

We thank E. V. Chulkov and P. M. Echenique for fruitful discussions and gratefully acknowledge funding by the Deutsche Forschungsgemeinschaft through SPP1093 and GK790 and by the Ikerbasque foundation.

[1] A. G. Borisov, J. P. Gauyacq, A. K. Kazansky, E. V. Chulkov, V. M. Silkin, and P. M. Echenique, Phys. Rev. Lett. **86**, 488 (2001).
[2] A. Föhlisch, P. Feulner, F. Hennies, A. Fink, D. Menzel, D. Sanchez-Portal, P. M. Echenique, and W. Wurth, Nature (London) **436**, 373 (2005).
[3] A. G. Borisov, V. Sametoglu, A. Winkelmann, A. Kubo, N. Pontius, J. Zhao, V. M. Silkin, J. P. Gauyacq, E. V. Chulkov, P. M. Echenique, and H. Petek, Phys. Rev. Lett. **101**, 266801 (2008).
[4] P. M. Echenique and J. B. Pendry, J. Phys. C **11**, 2065 (1978).
[5] T. Fauster and W. Steinmann, in *Electromagnetic Waves: Recent Developments in Research*, edited by P. Halevi (North-Holland, Amsterdam, 1995), Vol. 2, pp. 347–411.
[6] P. M. Echenique, R. Berndt, E. V. Chulkov, T. Fauster, A. Goldmann, and U. Höfer, Surf. Sci. Rep. **52**, 219 (2004).
[7] A. Goldmann, V. Dose, and G. Borstel, Phys. Rev. B **32**, 1971 (1985).
[8] E. V. Chulkov, V. M. Silkin, and P. M. Echenique, Surf. Sci. **437**, 330 (1999).
[9] R. W. Schoenlein, J. G. Fujimoto, G. L. Eesley, and T. W. Capehart, Phys. Rev. B **43**, 4688 (1991).
[10] R. L. Lingle, N. H. Ge, R. E. Jordan, J. D. McNeill, and C. B. Harris, Chem. Phys. **205**, 191 (1996); **208**, 297(E) (1996).
[11] C. B. Harris, N. H. Ge, R. L. Lingle, J. D. McNeill, and C. M. Wong, Annu. Rev. Phys. Chem. **48**, 711 (1997).
[12] M. Wolf, E. Knoesel, and T. Hertel, Phys. Rev. B **54**, R5295 (1996).
[13] M. Weinelt, J. Phys. Condens. Matter **14**, R1099 (2002).
[14] A. Damm, K. Schubert, J. Güdde, and U. Höfer, Phys. Rev. B **80**, 205425 (2009).
[15] M. Winter, E. V. Chulkov, and U. Höfer, Phys. Rev. Lett. **107**, 236801 (2011).
[16] A. G. Borisov, E. V. Chulkov, and P. M. Echenique, Phys. Rev. B **73**, 073402 (2006).
[17] U. Höfer, I. L. Shumay, C. Reuß, U. Thomann, W. Wallauer, and T. Fauster, Science **277**, 1480 (1997).
[18] I. L. Shumay, U. Höfer, C. Reuß, U. Thomann, W. Wallauer, and T. Fauster, Phys. Rev. B **58**, 13974 (1998).
[19] U. Höfer, Appl. Phys. B **68**, 383 (1999).
[20] C. Reuß, I. L. Shumay, U. Thomann, M. Kutschera, M. Weinelt, T. Fauster, and U. Höfer, Phys. Rev. Lett. **82**, 153 (1999).
[21] W. Berthold, P. Feulner, and U. Höfer, Chem. Phys. Lett. **358**, 502 (2002).
[22] W. Berthold, F. Rebentrost, P. Feulner, and U. Höfer, Appl. Phys. A **78**, 131 (2004).
[23] C. H. Schwalb, S. Sachs, M. Marks, A. Scholl, F. Reinert, E. Umbach, and U. Höfer, Phys. Rev. Lett. **101**, 146801 (2008).
[24] S. Sachs, C. H. Schwalb, M. Marks, A. Schöll, F. Reinert, E. Umbach, and U. Höfer, J. Chem. Phys. **131**, 144701 (2009).
[25] N. Pontius, V. Sametoglu, and H. Petek, Phys. Rev. B **72**, 115105 (2005).
[26] A. Winkelmann, V. Sametoglu, J. Zhao, A. Kubo, and H. Petek, Phys. Rev. B **76**, 195428 (2007).
[27] F. Reinert, G. Nicolay, S. Schmidt, D. Ehm, and S. Hüfner, Phys. Rev. B **63**, 115415 (2001).
[28] T. Klamroth, P. Saalfrank, and U. Höfer, Phys. Rev. B **64**, 035420 (2001).
[29] M. Rohleder, K. Duncker, W. Berthold, J. Güdde, and U. Höfer, New. J. Phys. **7**, 103 (2005).
[30] S. Ogawa, H. Nagano, and H. Petek, Phys. Rev. B **55**, 10869 (1997).
[31] S. Pawlik, M. Bauer, and M. Aeschlimann, Surf. Sci. **377**, 206 (1997).
[32] E. Knoesel, A. Hotzel, and M. Wolf, Phys. Rev. B **57**, 12812 (1998).
[33] R. Knorren, K. H. Bennemann, R. Burgermeister, and M. Aeschlimann, Phys. Rev. B **61**, 9427 (2000).
[34] H. Petek, H. Nagano, M. J. Weida, and S. Ogawa, Chem. Phys. **251**, 71 (2000).
[35] H. Petek and S. Ogawa, Prog. Surf. Sci. **56**, 239 (1997).
[36] E. Knoesel, A. Hotzel, and M. Wolf, J. Electron Spectrosc. Relat. Phenom. **88**, 577 (1998).
[37] M. Weinelt, C. Reuß, M. Kutschera, U. Thomann, I. L. Shumay, T. Fauster, U. Höfer, F. Theilmann, and A. Goldmann, Appl. Phys. B **68**, 377 (1999).

[38]H. Petek, A. P. Heberle, W. Nessler, H. Nagano, S. Kubota, S. Matsunami, N. Moriya, and S. Ogawa, Phys. Rev. Lett. **79**, 4649 (1997).
[39]S. Ogawa, H. Nagano, H. Petek, and A. P. Heberle, Phys. Rev. Lett. **78**, 1339 (1997).
[40]H. Petek, H. Nagano, and S. Ogawa, Phys. Rev. Lett. **83**, 832 (1999).
[41]J. Güdde, M. Rohleder, and U. Höfer, Appl. Phys. A **85**, 345 (2006).
[42]K. Boger, M. Roth, M. Weinelt, T. Fauster, and P. G. Reinhard, Phys. Rev. B **65**, 075104 (2002).
[43]J. Güdde, M. Rohleder, T. Meier, S. W. Koch, and U. Höfer, Science **318**, 1287 (2007).
[44]T. Fauster, M. Weinelt, and U. Höfer, Prog. Surf. Sci. **82**, 224 (2007).
[45]A. García-Lekue, J. M. Pitarke, E. V. Chulkov, A. Liebsch, and P. M. Echenique, Phys. Rev. B **68**, 045103 (2003).
[46]N. V. Smith, Phys. Rev. B **32**, 3549 (1985).
[47]P. M. Echenique, J. M. Pitarke, E. Chulkov, and V. M. Silkin, J. Electron Spectrosc. Relat. Phenom. **126**, 163 (2002).
[48]A. Liebsch, Phys. Rev. Lett. **71**, 145 (1993).
[49]A. Liebsch, Phys. Rev. B **48**, 11317 (1993).
[50]A. García-Lekue, J. M. Pitarke, E. V. Chulkov, A. Liebsch, and P. M. Echenique, Phys. Rev. Lett. **89**, 096401 (2002).
[51]K. Giesen, F. Hage, F. J. Himpsel, H. J. Riess, and W. Steinmann, Phys. Rev. Lett. **55**, 300 (1985).
[52]M. Rohleder, K. Duncker, W. Berthold, J. Güdde, and U. Höfer, Appl. Phys. A **88**, 527 (2007).
[53]J. Osma, I. Sarría, E. V. Chulkov, J. M. Pitarke, and P. M. Echenique, Phys. Rev. B **59**, 10591 (1999).
[54]W. Berthold, J. Güdde, P. Feulner, and U. Höfer, Appl. Phys. B **73**, 865 (2001).
[55]M. Roth, M. T. Pickel, W. Jinxiong, M. Weinelt, and T. Fauster, Phys. Rev. Lett. **88**, 096802 (2002).
[56]E. V. Chulkov, I. Sarría, V. M. Silkin, J. M. Pitarke, and P. M. Echenique, Phys. Rev. Lett. **80**, 4947 (1998).
[57]P. M. Echenique, J. M. Pitarke, E. V. Chulkov, and A. Rubio, Chem. Phys. **251**, 1 (2000).
[58]T. Fauster, C. Reuss, I. L. Shumay, and M. Weinelt, Chem. Phys. **251**, 111 (2000).
[59]M. Muntwiler and X. Y. Zhu, New J. Phys. **10**, 113018 (2008).